

Diffraction Optics for Moon Topography Mapping

John G. Smith^a, Luis Ramos-Izquierdo^b, Andrew Stockham^a, Stan Scott^b

^aMEMS Optical*, Inc., 205 Import Circle, Huntsville, AL, USA 35806

^bNASA Goddard Space Flight Center[†], Greenbelt, MD, USA 20771

ABSTRACT

This paper presents the design, analysis, and testing of a diffractive optical element (DOE) to be part of the Lunar Orbiter Laser Altimeter (LOLA) instrument scheduled to launch in 2008. LOLA will be one of six instruments to orbit the Moon for a year or more as part of the Lunar Reconnaissance Orbiter (LRO). The various scientific instruments aboard the LRO will map the lunar environment in greater detail than ever before. LOLA will produce a topographic map of the Moon from a nominal 50km orbit during the one-year mission. LOLA works by bouncing laser pulses off the lunar surface as it orbits the Moon. By measuring the time it takes for light to travel to the surface and back, LOLA can calculate the roundtrip distance. Each pulse consists of five laser spots in a cross-like pattern spanning about 50 meters of the lunar surface. The spots are generated by a DOE from the single, collimated LOLA laser input beam. It is projected that LOLA will gather more than a billion measurements of the Moon's surface elevation creating a high resolution three-dimensional map of the surface.

Keywords: diffractive optics, Lunar Orbiter Laser Altimeter, laser, topography, grayscale lithography, LIDAR

1.0 Introduction

The Lunar Orbiter Laser Altimeter (LOLA) is one of six remote sensing instruments scheduled to fly to the Moon in 2008 on board NASA's Lunar Reconnaissance Orbiter (LRO) spacecraft. LRO is the first mission of the Robotic Lunar Exploration Program (RLEP), a new NASA initiative designed to prepare the way for human return to the Moon. The three main exploration goals of LRO are to map potential landing sites, search for water and other lunar resources, and characterize the radiation environment that humans living on the Moon would have to contend with. The six LRO instruments, along with the technology demonstration of a miniature synthetic aperture radar (Mini-SAR), will work jointly during the one year mission to meet these three goals. LOLA's main role is to measure the topography, slope, and surface roughness of the Moon to the centimeter level from the nominal 50km mapping orbit. Differences in lunar reflectance at the 1064nm laser output wavelength will also allow LOLA to indicate potential locations of surface ice in the deep, shadowed regions of the lunar poles.

The LOLA instrument, shown in Figure 1, has direct heritage from the Mercury Laser Altimeter¹ (MLA), a Goddard Space Flight Center (GSFC) instrument currently on its way to Mercury on-board NASA's MESSENGER spacecraft. One of the main differences between MLA and LOLA is that LOLA is a multi-channel instrument while MLA has only a single channel. LOLA produces five laser beams that are mapped to five independent receiver detectors, and the signals processed independently to calculate the time-of-flight for each beam. The multiple LOLA channels will increase coverage at the Moon and will provide better surface slope and roughness information than possible with a single beam. The five output laser beams of LOLA are generated by a custom-designed diffractive optic element (DOE) located in collimated space at the output of the 18X LOLA laser beam expander. The DOE performs an almost equal energy split of the input laser beam and produces a cross-pattern in the far-field with the outer beams separated by 500 μ rad from a center, un-deviated beam. The DOE is the key technology that allows the straightforward generation of multiple output laser beams from a single laser input beam.

* info@memsoptical.com; phone 1 256 859-1886; fax 1 256 859-5890; www.memsoptical.com

[†] Luis.A.Ramos-Izquierdo@nasa.gov; phone 1 301 614 6745; fax 1 301614 6744; www.gsfc.nasa.gov

Copyright 2006 Society of Photo-Optical Instrumentation Engineers.

This paper was published in SPIE Proceedings Micro (MEMS) and Nanotechnologies for Space Applications and is made available as an electronic preprint with permission of SPIE. One print or electronic copy may be made for personal use only. Systematic or multiple reproduction, distribution to multiple locations via electronic or other means, duplication of any material in this paper for a fee or for commercial purposes, or modification of the content of the paper are prohibited.

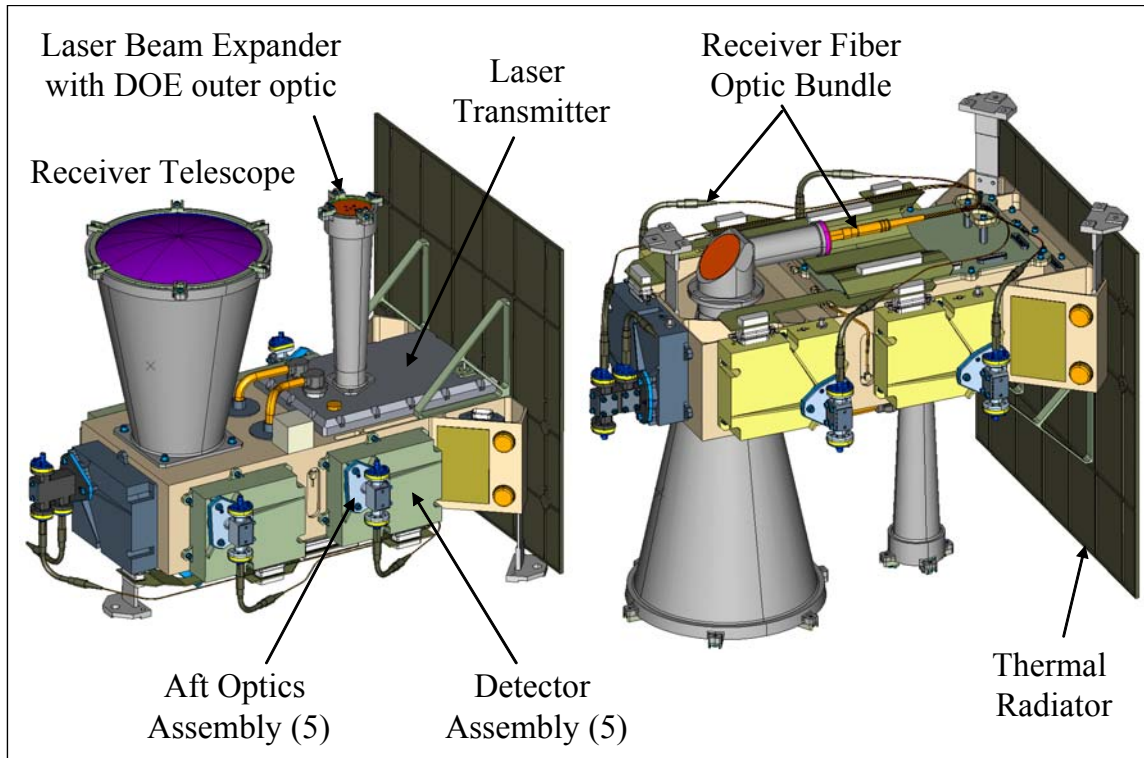


Figure 1. Instrumentation comprising LOLA.

2.0 DOE Design Specifications

In order for the DOE to provide a viable solution for the LOLA Transmitter optical system it has to meet critical performance and environmental requirements. The DOE must be efficient, lightweight, and rugged, and it must be able to operate in the space flight environment of the LOLA mapping orbit. The design requirements for the LOLA DOE are listed in Table 1. The key functional specifications are the overall efficiency and beam-to-beam energy uniformity, the precise $500\mu\text{rad}$ angular deviation of each of the four outer beams relative to the center beam, and the preservation of the input beam laser far-field divergence on each of the five diffracted beams. In addition, the DOE output pattern must be insensitive to DOE XYZ translations, tilts (except rotation about the optical axis), pressure changes, and temperature changes. The LOLA DOE is a custom design to operate with the expected LOLA laser output beam parameters: 1064.3nm wavelength, Gaussian TEM_{00} mode, 18mm $1/e^2$ diameter, $100\mu\text{rad}$ $1/e^2$ full-angle divergence, 2.7mJ pulse energy, 6nsec pulse width, and 28 Hz repetition rate.

3.0 Design and Analysis

Two theoretical designs were performed and evaluated against the specifications given in Table 1. The first design analyzed was on-axis where the un-diffracted beam, also known as the zero order, is part of the desired five orders. The second design analyzed was off-axis where the desired five orders is shifted away from the zero order. Off-axis designs allow for the best beam-to-beam uniformity². Fabrication errors typically cause the zero order to have a higher percentage of the energy. By designing the beam splitting DOE to be off-axis, the zero order is not part of the design making the design insensitive to fabrication errors. The main disadvantage of an off-axis design is the additional alignment having to do with the desired pattern being away from the optical axis.

Copyright 2006 Society of Photo-Optical Instrumentation Engineers.

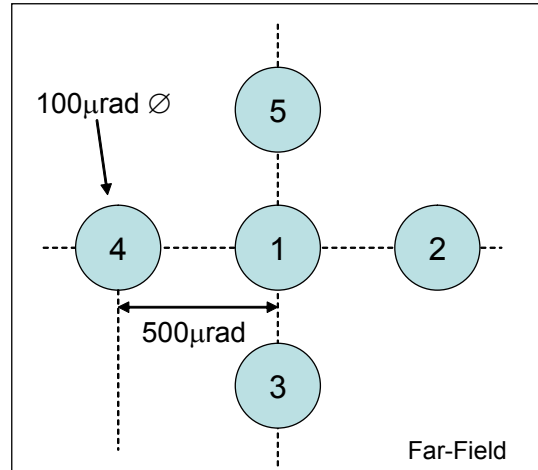
This paper was published in SPIE Proceedings Micro (MEMS) and Nanotechnologies for Space Applications and is made available as an electronic preprint with permission of SPIE. One print or electronic copy may be made for personal use only. Systematic or multiple reproduction, distribution to multiple locations via electronic or other means, duplication of any material in this paper for a fee or for commercial purposes, or modification of the content of the paper are prohibited.

Table 1. Design Specifications for the LOLA DOE.

Substrate	Corning 7980 Fused Silica
Size	40mm dia. x 4mm CT
Diffraction Efficiency	> 80% of input beam
Energy Uniformity	< 20% variation per beam
Beam Divergence	< 10 μ rad increase
Operating Environment	20C \pm 40C, 0ATM, 50krad's
Storage Environment	20C \pm 5C, 1ATM, 20-80% RH

Beam #	Far-Field Angular Coordinates		Reference
	X	Y	
1	0 \pm 250	0 \pm 250	Input Beam
2	500 \pm 20/-0	0 \pm 20	DOE Beam 1
3	0 \pm 20	-500 \pm 20/-0	DOE Beam 1
4	-500 \pm 20/-0	0 \pm 20	DOE Beam 1
5	0 \pm 20	500 \pm 20/-0	DOE Beam 1

Units in μ rad



3.1 Design and Background of Beam Splitting DOEs

Diffraction beam splitters are formed by etching a very shallow structure of a certain shape into the surface of a transparent material. Diffraction beam splitters are also referred to as phase gratings since this shallow structure alters the phase of the incoming wave to produce the desired far field pattern. The depth of the structure is typically equal to or less than one wave of optical path difference for a given material at a given wavelength of light. The structure is typically periodic and thus can be modeled by a Fourier analysis². Figure 2 is a diagram that shows the relationship between the incoming and outgoing beams.

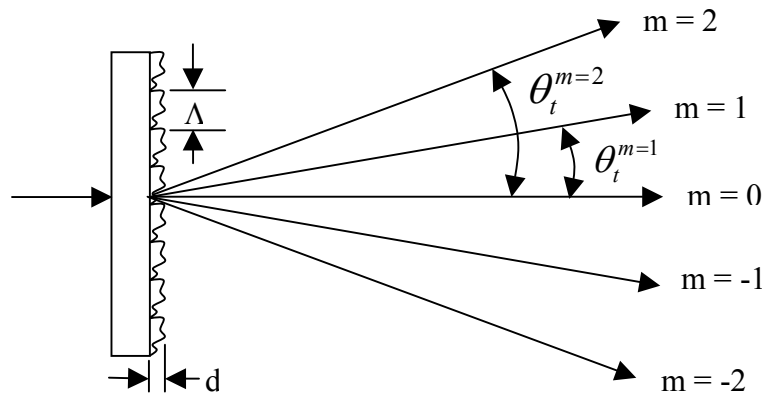


Figure 2. Sketch of grating with diffractive orders.

The grating equation provides the mathematical relationship for the angular separation of the orders for a beam incident normal to the grating:

$$\sin(\theta_t^m) = \frac{m\lambda}{\Lambda} \quad (1)$$

where θ_t^m is the angle from the surface normal, m is the diffractive order number, Λ is the period of the grating, and λ is the wavelength of the light. Equation 2 gives the typical one-wave depth for a phase grating structure

Copyright 2006 Society of Photo-Optical Instrumentation Engineers.

This paper was published in SPIE Proceedings Micro (MEMS) and Nanotechnologies for Space Applications and is made available as an electronic preprint with permission of SPIE. One print or electronic copy may be made for personal use only. Systematic or multiple reproduction, distribution to multiple locations via electronic or other means, duplication of any material in this paper for a fee or for commercial purposes, or modification of the content of the paper are prohibited.

$$d = \frac{\lambda}{n-1} \quad (2)$$

where d is the etch depth and n is the index of refraction for the material into which the grating will be etched. For the LOLA DOE, the period is $2128.6\mu\text{m}$. The theoretical depth at $1.0643\mu\text{m}$ in fused silica is $2.366\mu\text{m}$. The mathematical operation of the grating convolves the input beam with the spatial frequencies defined by the surface relief structure of the grating. The result, shown in Figure 3, is the input beam copied to each angular location (diffractive order) and scaled by the weighting of that diffractive order.

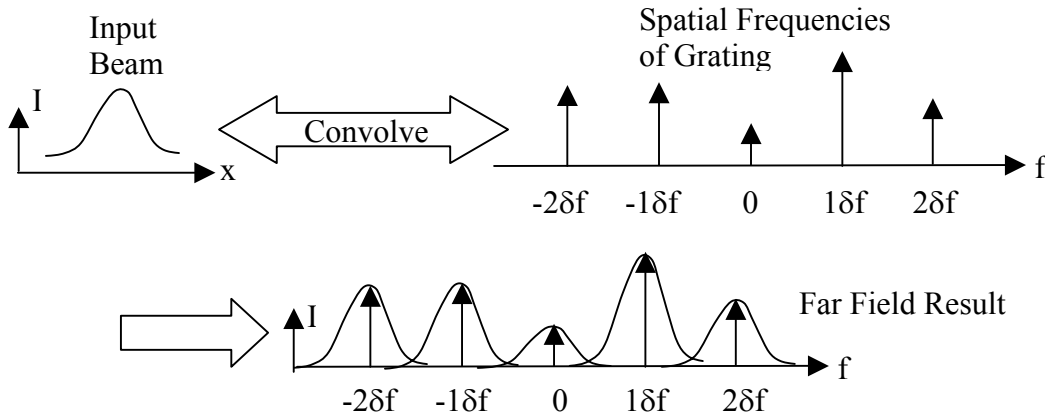
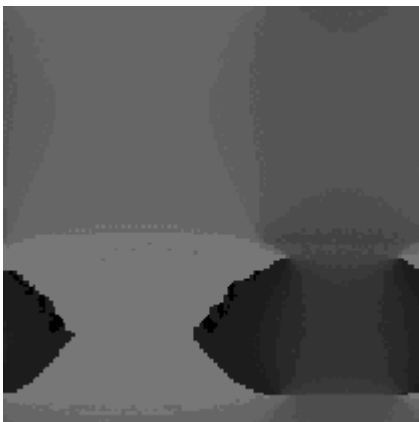
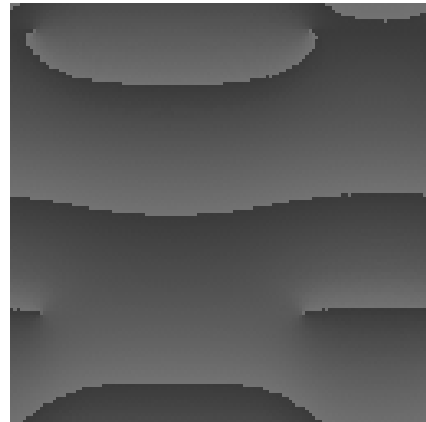


Figure 3. Operation of the grating is to make scaled copies of the input beam at each diffraction order.

The specific details of the surface topography of the grating can be very non-intuitive. Thus, many robust design techniques such as genetic algorithms, simulated annealing, and a variety of other algorithms have been developed to iteratively arrive at an optimal solution. Figure 4 shows one period for each design, on-axis and off-axis, for the LOLA DOE.



(a) Surface relief profile of one period of the on-axis design.



(b) Surface relief profile of one period of the off-axis design.

Figure 4. One period of each design.

The fabrication of these micro-structures in the surface of the material can be accomplished several different ways. The most common method is to use a photolithography step followed by an etching step as is done in the semiconductor

Copyright 2006 Society of Photo-Optical Instrumentation Engineers.

This paper was published in SPIE Proceedings Micro (MEMS) and Nanotechnologies for Space Applications and is made available as an electronic preprint with permission of SPIE. One print or electronic copy may be made for personal use only. Systematic or multiple reproduction, distribution to multiple locations via electronic or other means, duplication of any material in this paper for a fee or for commercial purposes, or modification of the content of the paper are prohibited.

manufacturing industry. The two main methods for the photolithography are to use a series of binary masks to build a stepped multiphase structure or a single gray scale mask to create a near continuous structure. Typically, the grayscale mask technique produces a higher quality result with fewer fabrication steps and thus less cost. The LOLA DOE was produced at MEMS Optical, Inc. using their patented grayscale technology⁴.

3.2 Fabrication Tolerance Analysis

Once the surface relief profiles were designed through computer optimization, a tolerance analysis was performed to see the impact on diffraction efficiency and uniformity. The uniformity is defined based on the intensity in each diffracted order:

$$U = \frac{I_{\max} - I_{\min}}{2 \cdot \text{Avg}} \quad (3)$$

The theoretical designs shown in Figure 4 were greater than 84% efficient and showed a beam-to-beam uniformity less than 1%. Figure 5 shows the effect on efficiency due to etch depth error, and Figure 6 shows the effect on uniformity.

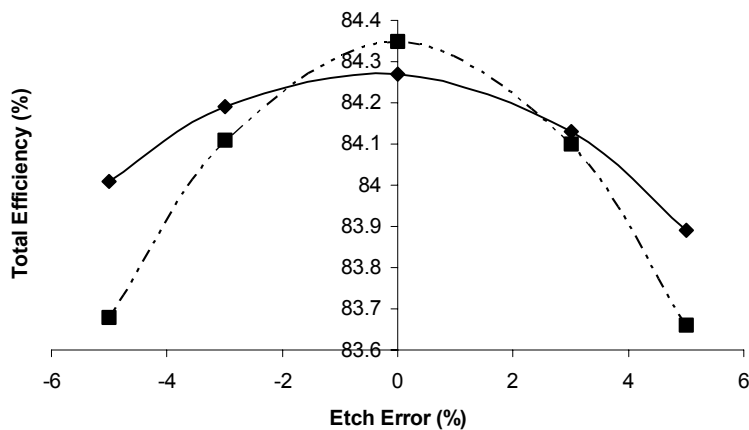


Figure 5. On-axis design (solid) and the off-axis design (dashed).

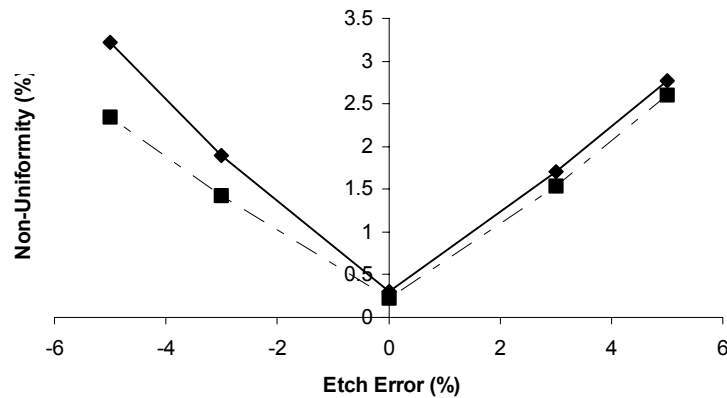


Figure 6. On-axis design (solid) and the off-axis design (dashed).

As can be seen from Figures 5 and 6 with a typical etch depth error of $\pm 5\%$, the on-axis design still meets the optical performance given in Table 1.

Copyright 2006 Society of Photo-Optical Instrumentation Engineers.

This paper was published in SPIE Proceedings Micro (MEMS) and Nanotechnologies for Space Applications and is made available as an electronic preprint with permission of SPIE. One print or electronic copy may be made for personal use only. Systematic or multiple reproduction, distribution to multiple locations via electronic or other means, duplication of any material in this paper for a fee or for commercial purposes, or modification of the content of the paper are prohibited.

3.3 Alignment Sensitivity

A diffraction grating with a period of 2129 μm was modeled in ZEMAX[®] to determine its sensitivity to alignment errors. A simple thin lens with a focal length of 100mm was placed behind the grating to observe the angular displacement of the diffraction pattern as it was tilted at various field angles. Figure 7 gives a plot of the results. The specification was for the change in the pattern angles to be less than 10 μrad at a tilt angle of 0.1°. Based upon the ZEMAX[®] modeling, the angular displacement of the diffraction pattern was 0.3 picoradians at a tilt angle of 0.1°.

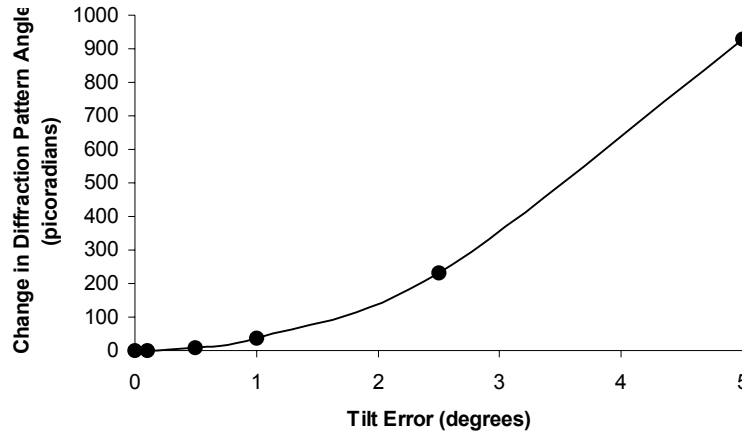


Figure 7. Angular sensitivity plot showing the angular displacement of the diffraction pattern in response to alignment errors due to tilt.

3.3 Environmental Issues

The linear fractional expansion of the component when taken to zero pressure can be approximately determined with the following formula:

$$\Delta l \approx \frac{1}{3} \frac{\Delta p}{B} \quad (1)$$

where Δp is the change in pressure and B is the bulk modulus of the material. For fused silica, the bulk modulus is 35.4GPa, which results in a linear expansion of 9.4×10^{-7} . The effect upon the LOLA Laser beam splitter will be an increase of the period, which in turn will slightly alter the diffraction angle. Using the grating equation and a new period of 2128.6002 μm , the new diffraction angle will be 499.99995 μrad , so pressure change results in negligible effect to the grating performance.

The operating temperature of -60°C to $+60^\circ\text{C}$ will result in a change of the index of refraction of the material. ZEMAX[®] gave the following indices of refraction for fused silica for the given temperature and pressure ranges.

Table 2. Change in the index of refraction.

Temperature	Pressure	
	0 ATM	1 ATM
-60°C	1.4596	1.4589
$+60^\circ\text{C}$	1.4607	1.4603

However, the percent error for the index will be 0.18%. The divergence angle is not dependent on the index of refraction. The temperature change will result in thermal expansion of the material. The Corning specification for fused silica lists an average CTE of 0.48ppm/K for the temperature range of -100°C to $+200^\circ\text{C}$. Since the part will be

Copyright 2006 Society of Photo-Optical Instrumentation Engineers.

This paper was published in SPIE Proceedings Micro (MEMS) and Nanotechnologies for Space Applications and is made available as an electronic preprint with permission of SPIE. One print or electronic copy may be made for personal use only. Systematic or multiple reproduction, distribution to multiple locations via electronic or other means, duplication of any material in this paper for a fee or for commercial purposes, or modification of the content of the paper are prohibited.

made at 20°C, a minimum and maximum change in length will occur for going from 20°C to -60°C and then from 20°C to 60°C, respectively. Using the below equation, the extreme limits of the expansion can be calculated

$$\varepsilon = \alpha\Delta T \quad (2)$$

where ε is the strain, α is the CTE of the material, and ΔT is the change in temperature. The minimum strain will be 38.4×10^{-6} , and the maximum will be 19.2×10^{-6} . Using the grating equation and a new period for each case of $2128.682 \mu\text{m}$ and $2128.641 \mu\text{m}$, the new diffraction angles will be $499.83981 \mu\text{rad}$ and $499.99037 \mu\text{rad}$.

4.0 DOE Prototype Testing

To validate the theoretical design of the DOE, a set of calibration wafers were fabricated and tested at NASA/GSFC in the summer of 2004. The wafers were tested with a Nd:YAG laser that closely matched the output beam specifications of the LOLA flight laser. The 100mm diameter calibration wafers were divided into three sections with different etch depths. The goal of this initial test program was to validate the design of the DOE, and to select the optimum etch depth for fabrication of DOE prototypes of the correct physical size. All three sections of the calibration wafer produced the required far-field diffraction pattern, but the etch depth proved to be a very sensitive parameter affecting the energy balance between the five diffracted beams. The far-field image of the input laser beam and the resulting diffraction pattern with the DOE in the path is shown in Figure 8. The DOE image is saturated by ~3X to bring out the higher order diffraction modes. A cross-section of the DOE far-field image for the three different etch depths is shown in Figure 9. The plot is normalized to unity at the peak of the center beam for ease of comparison.

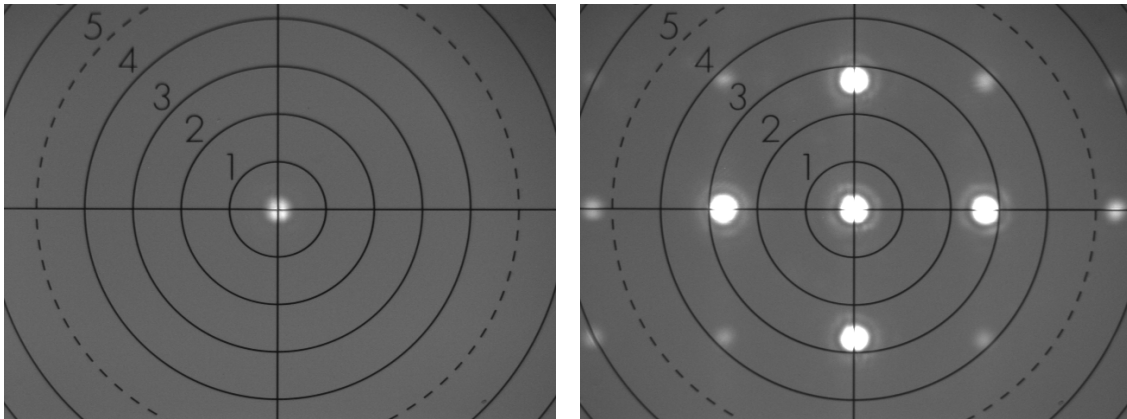


Figure 8. Far-field images: Input beam (left) and DOE (right, ~3X saturation).

Once the optimum etch depth was established, seven DOE prototypes were fabricated, one of which is shown in Figure 10. Two of the prototypes were uncoated, two were AR coated on the optically smooth side only, and three were AR coated on both sides to maximize DOE efficiency. The prototypes had these different AR coating configurations because NASA wanted to verify that AR coating the fine etched diffraction features would not affect the efficiency, diffraction angle, or wavefront error of the DOE's. This proved to be the case and through testing showed >99% efficiency in the near-field (at the output of the DOE), and >80% efficiency of the five diffracted beams in the far-field (the rest of the energy goes to the higher order diffraction modes) with the DOE prototypes AR coated on both sides. The angular separation of the four outer beams was measured with a theodolite on all seven prototypes, and the angles were found to be within 1% of the required $500 \mu\text{rad}$ design value. The DOE prototypes also preserved the input beam $100 \mu\text{rad}$ divergence on all five diffracted beams to within our measurement accuracy of $\sim 10 \mu\text{rad}$. The DOE prototypes were then placed in vacuum and thermal chambers to confirm that the beam energy, beam angle, and beam divergence were not affected by the operating environment. NASA also verified that small translations ($\sim 1 \text{mm}$) and small tilts ($\sim 1^\circ$) did not affect the DOE output beam parameters.

Copyright 2006 Society of Photo-Optical Instrumentation Engineers.

This paper was published in SPIE Proceedings Micro (MEMS) and Nanotechnologies for Space Applications and is made available as an electronic preprint with permission of SPIE. One print or electronic copy may be made for personal use only. Systematic or multiple reproduction, distribution to multiple locations via electronic or other means, duplication of any material in this paper for a fee or for commercial purposes, or modification of the content of the paper are prohibited.

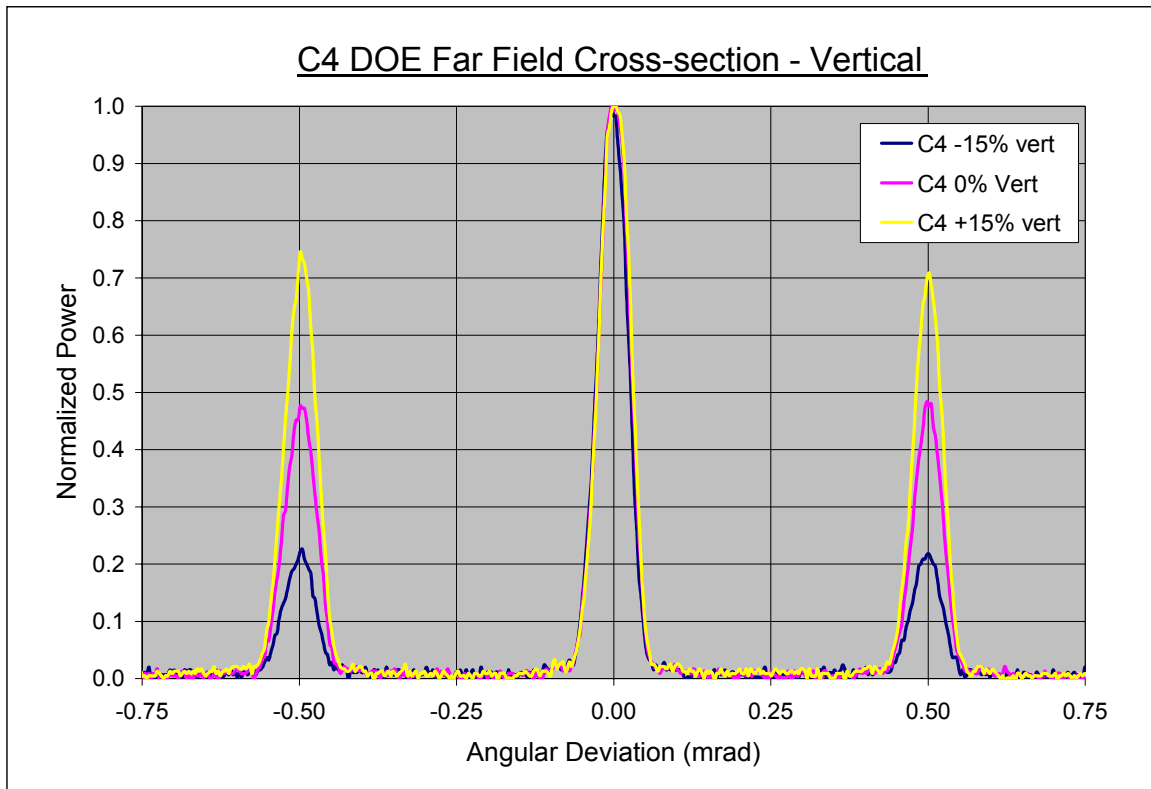


Figure 9. DOE calibration wafer far-field pattern cross-sections.

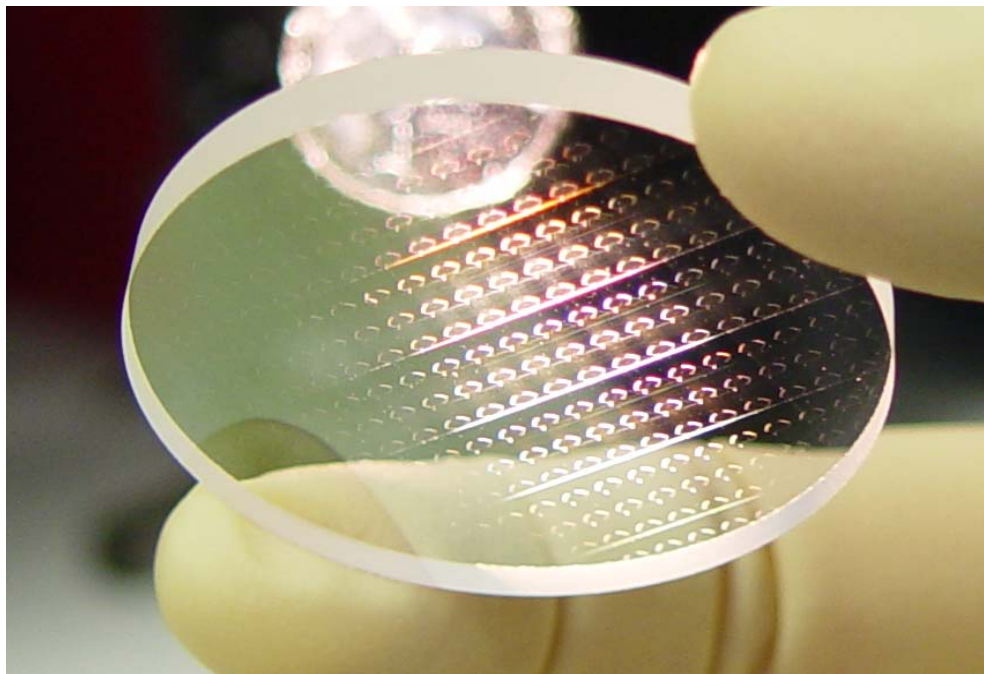


Figure 10. 40mm diameter and 4mm thick fused silica DOE prototype.

Copyright 2006 Society of Photo-Optical Instrumentation Engineers.

This paper was published in SPIE Proceedings Micro (MEMS) and Nanotechnologies for Space Applications and is made available as an electronic preprint with permission of SPIE. One print or electronic copy may be made for personal use only. Systematic or multiple reproduction, distribution to multiple locations via electronic or other means, duplication of any material in this paper for a fee or for commercial purposes, or modification of the content of the paper are prohibited.

The only specification that the DOE prototypes failed to meet was the beam-to-beam energy uniformity. Since the minimum feature size for the design is greater than $10\mu\text{m}$ and the material is fused silica, additional tolerancing of rounding of the features that can occur during the etching process was not modeled in the initial design phase. Figure 11 is a pictorial representation of what is met by rounding of features or blur.

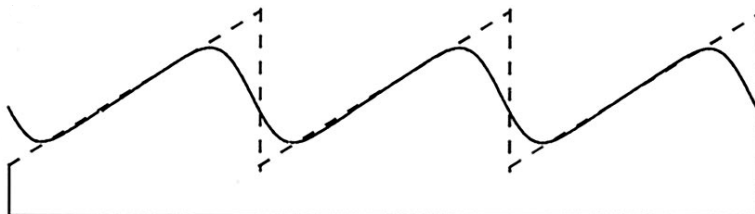


Figure 11. Rounding of the features during fabrication.

Additional modeling was performed to correlate the amount of rounding during fabrication to the test data. Figure 12 shows the uniformity not including the percentage of energy in the zero order for the modeling results and the test results. Figure 13 shows the amount of energy in the zero order for the modeling results and the test results.

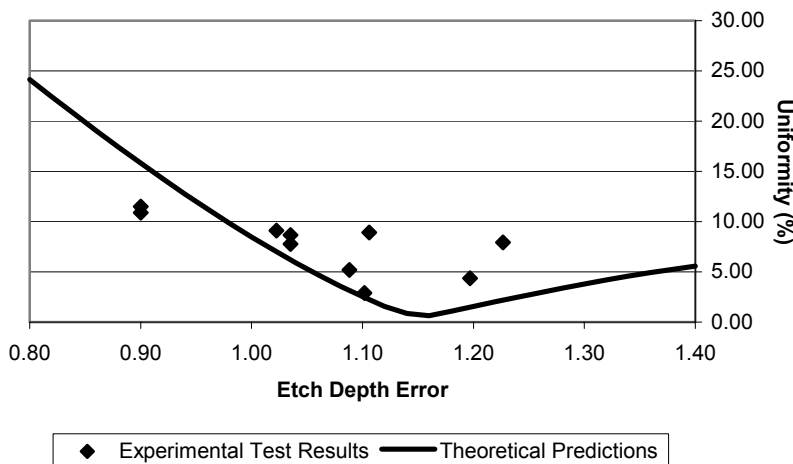


Figure 12. Uniformity versus etch depth error accounting for blur.

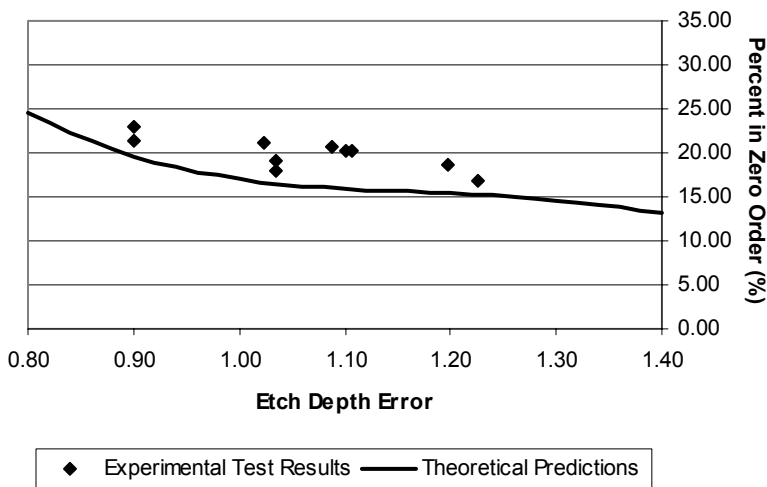


Figure 13. Percent in the zero order versus etch depth error accounting for blur.

Copyright 2006 Society of Photo-Optical Instrumentation Engineers.

This paper was published in SPIE Proceedings Micro (MEMS) and Nanotechnologies for Space Applications and is made available as an electronic preprint with permission of SPIE. One print or electronic copy may be made for personal use only. Systematic or multiple reproduction, distribution to multiple locations via electronic or other means, duplication of any material in this paper for a fee or for commercial purposes, or modification of the content of the paper are prohibited.

Another calibration wafer will be produced in the spring of 2006 to select more appropriate etch depths accounting for the rounding of the features. The final DOE parts will include an alignment notch at the edge of the part to prevent the DOE from rotating once it is installed in the LOLA laser beam expander tube.

5.0 Conclusion

The LOLA DOE prototype design, fabrication, and test program has shown that it is possible to meet the LOLA transmitter beam splitter requirements with a single, simple diffractive optic element. A new calibration wafer is currently under fabrication to finalize the optimum etch depth for the LOLA flight DOE. It is expected that this second fabrication and testing program will be completed early in the spring of 2006, and the flight DOE will be delivered shortly after that. An engineering model of the LOLA beam expander including a prototype DOE is currently underway so we can perform system level testing with the LOLA EM laser and instrument.

6.0 References

1. L. Ramos-Izquierdo, V. Scott III, S. Schmidt, J. Britt, W. Mamakos, R. Trunzo, J. Cavanaugh, and R. Miller, "Optical system design and integration of the Mercury Laser Altimeter," *Appl. Opt.* **44**, 1748-1760 (2005)
2. U.S. Patents 6,922,286 and 6,731,432
3. D. Brown, Chapter 6, "Beam Shaping with Diffractive Diffusers", F.M. Dickey and S.C. Holswade, *Laser Beam Shaping Theory and Techniques*, New York: Marcel Dekker, 2000
4. U.S. Patents 5,310,623 and 5,480,764

Copyright 2006 Society of Photo-Optical Instrumentation Engineers.

This paper was published in SPIE Proceedings Micro (MEMS) and Nanotechnologies for Space Applications and is made available as an electronic preprint with permission of SPIE. One print or electronic copy may be made for personal use only. Systematic or multiple reproduction, distribution to multiple locations via electronic or other means, duplication of any material in this paper for a fee or for commercial purposes, or modification of the content of the paper are prohibited.